arXiv:1607.03091v1 [astro-ph.GA] 11 Jul 2016

Model Predictions of the Results of Interferometric Observations for Stars under Conditions of Strong Gravitational Scattering by Black Holes and Wormholes

Alexander Shatskiy,[1] Yu. Yu. Kovalev,[2] and I. D. Novikov[2,3]

[1] *shatskiyalex@gmail.com*

[2] *Astro Space Center, Lebedev Physical Institute, Russian Academy of Sciences, Profsoyuznaya ul. 84/32, Moscow, 117997 Russia*

[3] *The Nielse Bohr International Academy, The Nielse Bohr Institute, Blegdamsvej 17, DK-2100 Copenhagen, Denmark*

The characteristic and distinctive features of the visibility amplitude of interferometric observations for compact objects like stars in the immediate vicinity of the central black hole in our Galaxy are considered. These features are associated with the specifics of strong gravitational scattering of point sources by black holes, wormholes, or black–white holes. The revealed features will help to determine the most important topological characteristics of the central object in our Galaxy: whether this object possesses the properties of only a black hole or also has characteristics unique to wormholes or black–white holes. These studies can be used to interpret the results of optical, infrared, and radio interferometric observations.

I. INTRODUCTION

Observations of many objects in the Universe with single telescopes, even space ones, do not allow their structure to be investigated, because their angular sizes are small. At the same time, the angular resolution of present day long baseline optical, infrared, and radio interferometers (the latter are the so called very long baseline interferometers, VLBI) approaches ten microarcseconds[1] see, for example, [see, for example, 1–6]). However, an interferometer records not the image of a compact object itself but its complex Fourier

[1] 1 microarcsecond (mas) $\approx 4.8 \cdot 10^{-12}$ rad.

transform V or, as it is also called the "visibility function" (see [1] for more details):

$$V(\mathrm{u},\mathrm{v}) = \int\int I(x,y)\exp\left[-2\pi i(\mathrm{xu}+\mathrm{yv})/\lambda\right]\,dx\,dy \tag{1}$$

Here, I is the intensity of the image; (x, y) are its angular coordinates; (u, v) are the coordinates of the interferometer baseline projection onto the (x, y) plane; and λ is the wavelength at which the fringe pattern is observed. The complex expression (1) has an amplitude and a phase (which is defined by the phase difference between the signal arrivals at the interferometer's telescopes). The inverse Fourier transform should be performed to synthesize the image from the Fourier transform:

$$I(x,y) = \int\int V(\mathrm{u},\mathrm{v})\exp\left[2\pi i(\mathrm{xu}+\mathrm{yv})/\lambda\right]\,\mathrm{du}\,\mathrm{dv} \tag{2}$$

As is well known (see, e.g., [1]), the phase is a no less important function than the amplitude when the image is reconstructed from the Fourier transform. Moreover, it is virtually impossible to properly reconstruct the image without knowing the phase. However, not all interferometers are able to measure the visibility function phase. In addition, real interferometric observations do not give a filled (u, v) plane, which makes it difficult to reconstruct the image of an object and limits the dynamic range of the resulting map. The method of directly modeling and comparing the results of visibility function amplitude (or Correlated Flux Density – CFD) measurements for the compact object being investigated and the model by the χ^2 minimization technique can be used to solve these problems. In this paper, we will attempt to find the characteristic features in the CFD for compact objects that can be associated with strong gravitational scattering of stars in the field of a black hole or wormhole. A similar approach is applied by the group of the Event Horizon Telescope (see [7, 8]). We will note at once that the stars we consider are bright, point, and compact objects that cannot be resolved. However, the stars can produce a system of fairly bright point images through strong gravitational scattering. This system will make a characteristic contribution to the CFD formation, because the sizes of this system of images will be large enough for its angular resolution with an interferometer but still insufficient for its observation with a single telescope. A thin shining ring that, according to theoretical predictions, must be seen around a Schwarzschild black hole (the apparent diameter of this ring in linear units is $3\sqrt{3}r_g/2$, where r_g is the gravitational radius) can be a typical example of such a system of images from stars close to a black hole.

As the main object of investigation we will choose the object at the center of our Milky Way, a massive black hole with a mass $\approx 4.3 \cdot 10^6 M_\odot$ and a gravitational radius $\approx 13 \cdot 10^6$ km (see, e.g., [9]).

The supermassive black hole in the quasar M87 with a mass of $\approx 3.4 \cdot 10^9 M_\odot$ (see, e.g., [8]) could be yet another possible candidate for an object of observation, because the angular size of the horizon radius for this black hole turns out to be sufficient ($r_g/r \approx 4.7\,\mu as \approx 2.3 \cdot 10^{-11}$ rad). However, with this quasar being too far away from us (≈ 16 Mpc), we cannot count on the detection of individual stars, including bright radio pulsars, with interferometers.

Since the effects being investigated are expected to be observed at the sensitivity limit of interferometers, for solar type stars it makes sense to consider infrared and optical observations, i.e., for $\lambda \sim 1\mu m$. It is in this range that the brightness of stars is at a maximum. However, an assumption about the pattern of the radiation spectrum for stars and background should also be made in the optical and infrared ranges (as, for example, was done in [8]). The point is that the relative width of the detected spectral band ($\Delta\lambda/\lambda$) is great in the optical and infrared ranges. For example, we can assume a flat spectrum or choose a spectrum typical of a solar type star.

In the radio band, VLBI systems record relatively narrow band signals, and there is no need to make any assumptions about the spectrum shape. However, the brightness of ordinary stars is insufficient, and pulsars can be considered in principle as the bright and point sources needed for us. Our subsequent calculations will be performed under the assumption of a monochromatic spectrum.

II. BRIGHTNESS VARIATIONS DURING THE PROPAGATION OF A THIN LIGHT BEAM

To avoid misunderstandings, we will note at once: by strong gravitational scattering we will mean not the brightness amplification in sources (as is usually meant when gravitational scattering is considered) but, on the contrary, the attenuation of their brightness through the scattering of light by the gravitational lens. Therefore, we will not be interested in the standard formulas and conclusions of gravitational scattering, where the observer is assumed to be almost in the focal plane of the lens. Since these are highly unlikely joint conditions for the source, the gravitational center, and the observer, quite the reverse is true in our

case: the observer is far from the focal plane of the lens. Indeed, only a very small fraction of celestial sources (from their total number) turn out to be gravitationally lensed by some bodies in the Universe for an observer on Earth.

Consider a thin light beam from a distant star propagating in a gravitational field. Suppose that the gravitational field is spherically symmetric and, therefore, the light beam propagates near a single plane (in which the source of the gravitational field lies). The beam parameters before gravitational scattering will be denoted by index "$_1$"; after gravitational scattering, an observer on Earth records the parameters of the starlight in the beam denoted by index "$_2$". Let the source be at a distance l_1 from the gravitational center and the observer be on Earth (at a distance l_2 from the gravitational center), with $l_1 << l_2$. For convenience, we will confine the light beam to a rectangular section, with the beam width in a direction parallel to the plane under consideration being assumed to be equal to db (see Fig. 1). Let the extreme rays of light along the beam width differ from one another by dh, where h is the impact parameter of the photons in the ray relative to the gravitational center (this is an integral of motion for a photon (see [10]). Since the gravitational field changes along the beam width, the width db changes due to the deviation of null geodesic photons in a non-uniform gravitational field. The beam width db_1 far from the gravitational center (before scattering) must coincide with dh. We assume the beam thickness in a direction orthogonal to the plane of the beam width to be equal to ξ.

All null geodesics (rays of light) with identical impact parameters converge at a single point after gravitational deflection and thereafter again begin to diverge (see, e.g., [11]).

Let $\varphi^{tot}(h)$ be the total photon deflection angle[2] (on the way from the source to the observer). In the most general spherically symmetric metric dependent only on the radial coordinate, this angle is defined by the expression (see [10]):

$$\varphi^{tot}(h) = 2 \int\limits_{r_{min}(h)}^{\infty} \frac{-h\,dr}{R^2\sqrt{f_r(1/f_t - h^2/R^2)}}\,, \quad R^2(r_{min}) = h^2 f_t(r_{min})\,. \tag{3}$$

The metric functions in this expression are defined by the metric

$$ds^2 = f_t(r)\,dt^2 - \frac{dr^2}{f_r(r)} - R^2(r)\,d\Omega^2\,, \quad d\Omega^2 := d\theta^2 + \sin^2\theta\,d\varphi^2\,. \tag{4}$$

For the Schwarzschild metric, for example, we have: $f_t = f_r = (1 - r_g/r)$, $R^2 = r^2$.

[2] The total photon deflection angle $\varphi^{tot}(h) > \pi$ is measured from the field center relative to the light source.

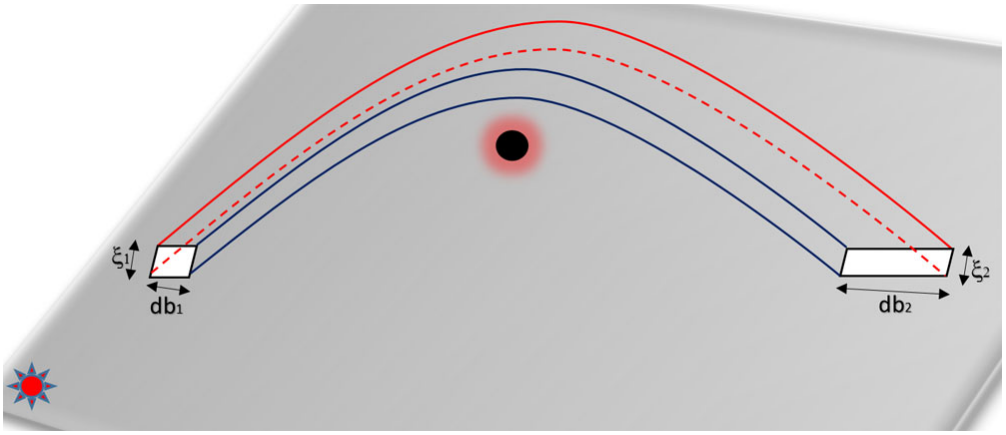

Figure 1: Schematic illustration of the propagation of a thin straight light beam in a spherically symmetric gravitational field. The distance from the central object to the source is assumed to be much smaller than the distance to the observer (Earth); the height and width of the beam change as it propagates in the gravitational field.

Since we will be interested in strong gravitational scattering (when the total change in light beam direction is greater than or approximately equal to $\sim \pi/2$), the point at which the rays again converge is at a distance $l_{eins} << l_2$ from the gravitating center. Consequently, the light beam parameters near the Earth are defined by the relations[3]:

$$\xi_2 = |\xi_1 \cdot (l_2/l_1) - l_2\, \xi_1\, (\sin \varphi^{tot})/h| \tag{5}$$

$$db_2 = |db_1 \cdot (l_2/l_1) + l_2\, \delta\varphi^{tot}| \approx |dh \cdot (l_2/l_1) - l_2 \partial_h \varphi^{tot}\, dh| \tag{6}$$

Under weak gravitational scattering of a massive body, we have $\partial_h \varphi^{tot} < 0$ and $\sin \varphi^{tot} < 0$; consequently, only the positive quantities are summed in Eqs. (5) and (6) for this case.

Since the total energy flux in the beam must be the same before and after its scattering by the gravitating center, the apparent brightness of light I in the beam must be inversely proportional to the cross-sectional area of the beam $dS := \xi\, db$, i.e., $I_2/I_1 = (\xi_1 db_1)/(\xi_2 db_2)$.

Let $I_2^{ordinary}$ be the intensity of light in the beam near the Earth that would be if there

[3] In Eqs. (5-6) we took into account the natural divergence of the light beam under consideration, i.e., the increase in the beam cross section dS unrelated to the gravitational field; this increase dS must be inversely proportional to the square of the distance from the star l, because $\xi \propto 1/l$ and $db \propto 1/l$ (these are the first terms on the right-hand sides of Eqs. (5-6). We also took into account the proportion following from the relation for the light cones before and after scattering: $\xi_1/h = \Delta\xi_2/(l_2 \sin \varphi^{tot})$.

was no gravitational field:

$$\frac{I_2^{ordinary}}{I_1} := \frac{l_1^2}{l_2^2} \tag{7}$$

This formula describes the natural divergence of the beam and the natural brightness attenuation in it.

Denote the coefficient of gravitational attenuation of the intensity in the beam by $\kappa := I_2/I_2^{ordinary}$. From Eqs. (5-7) for κ we then have

$$\kappa = \frac{1}{|(1 - l_1\partial_h\varphi^{tot})(1 - l_1 \sin\varphi^{tot}/h)|} \tag{8}$$

For the Schwarzschild metric, at large h (under weak gravitational scattering according to [12], §101), we have $\varphi^{tot} \approx \pi + 2r_g/h$, i.e., we obtain $\kappa \to 1$ at $h >> r_g$, as it must be.

Let us now estimate the strong gravitational scattering in the Schwarzschild metric for the stars nearest to the central black hole in our Galaxy. One of the stars nearest to the central black hole, S2 (in Sagittarius; see [9]), is at a distance of $\approx 18 \cdot 10^9 km$ from it ($\approx 1500 r_g$) and the attenuation coefficient for this star turns out to be $\kappa_{S2} \approx 3 \cdot 10^{-6}$ (at $\varphi^{tot} = 1.5\pi$).

Of course, an observer on Earth will see the source directly (with a natural brightness attenuation approximately equal to $\approx l_1^2/l_2^2$) and (hypothetically), after strong gravitational scattering, from a ring with a radius of about $3\sqrt{3}r_g/2$ around the central black hole, where the source's brightness near the Earth is defined by Eqs. (7) and (8). If there are quite a few such stars (at the very center of the Milky Way), then the entire ring with a radius of about $\sim 3\sqrt{3}r_g/2$ around the black hole turns out to be shining.

A star like our Sun placed at the center of the Milky Way will be seen as a star of approximately the 19th magnitude. Since a brightness attenuation by a million times corresponds to $\delta m = 15$, the Sun placed at the center of the Milky Way must be seen as a star of the 34th magnitude after the strong gravitational scattering considered above. This is still an unattainable sensitivity level for present-day telescopes. However, as is well known, there exist stars that have an absolute luminosity higher than the solar one by many orders of magnitude.

III. GRAVITATIONAL SCATTERING BY A BLACK–WHITE HOLE

In contrast to ordinary (external) gravitational scattering by a massive body, under internal gravitational scattering of light from another universe, the greater the h, the greater the

total photon deflection angle[4] φ^{tot} on the way from the source to the observer. Since φ^{tot} can be zero (at $h = 0$) and the derivative $\partial_h \varphi^{tot}$ can be positive, the light attenuation coefficient κ_{wh} for a wormhole or black–white hole can generally be arbitrary (large, small, or of the order of unity)! This makes it possible to see the light of stars from another universe and to distinguish it from the light of stars in our Universe.

Consider the main properties of strong gravitational scattering by a wormhole [13] or black–white hole [10]. Each point source in the Universe from the black hole will be seen as an infinite number of images in the Universe from the white hole. In this case, each image corresponds to its impact parameter h. The two main images of the source correspond to the total photon deflection through angles $\varphi_1^{tot} < 2\pi$ and $\varphi_{1'}^{tot} = 2\pi - \varphi_1^{tot}$, implying that the photons go around the center on different sides (these two images will be seen on the same line with the center and on different sides from it). The next two images (with larger impact parameters h) correspond to the photon deflection angles $\varphi_2^{tot} = 2\pi + \varphi_1^{tot}$ and $\varphi_{2'}^{tot} = 2\pi + \varphi_{1'}^{tot}$. The next pair is $\varphi_3^{tot} = 4\pi + \varphi_1^{tot}$ and $\varphi_{3'}^{tot} = 4\pi + \varphi_{1'}^{tot}$. And so on.

We considered two models: a Bronnikov–Ellis wormhole (see [14, 15]) and a Reissner–Nordstrom black–white hole (see [10]). For the model of a Bronnikov–Ellis wormhole, the metric is written as

$$ds^2 = (1 - r_g/R)\, dt^2 - dr^2 - R^2\, d\Omega^2, \quad R^2 := r^2 + r_0^2, \quad r_g < r_0. \tag{9}$$

In this model, for the maximum impact parameter of a photon that passes from another universe into our Universe, we have $h_{max} = r_g\sqrt{27}/2$ (at $\frac{2}{3}r_0 < r_g < r_0$) and $h_{max} = r_0^{3/2}/\sqrt{r_0 - r_g}$ (at $r_g \le \frac{2}{3}r_0$).

For $r_g = 0$ and $h \to 0$, we have the asymptotics $\varphi^{tot}(h) \to \pi h/r_0$ and, therefore, $\kappa_{wh}(h) \to r_0^2/(2\pi l_1^2)$; in a more general case ($r_g > 0$), the asymptotics of κ_{wh} does not depend on h either (see [13]). For the model of a Reissner–Nordstrom black–white hole,

$$ds^2 = f(r)\, dt^2 - f^{-1}(r)\, dr^2 - r^2\, d\Omega^2, \quad f(r) := \left(1 - \frac{r_c}{r}\right)\left(1 - \frac{r_h}{r}\right). \tag{10}$$

In this case, the charge of the black hole is $Q = \sqrt{r_c r_h}$ and its mass is $M = (r_c + r_h)/2$, where r_c and r_h are the inner and outer horizon radii.

---

[4] The passage of the ray with $h = 0$ corresponds (by definition) to rectilinear propagation of the ray of light in a wormhole.

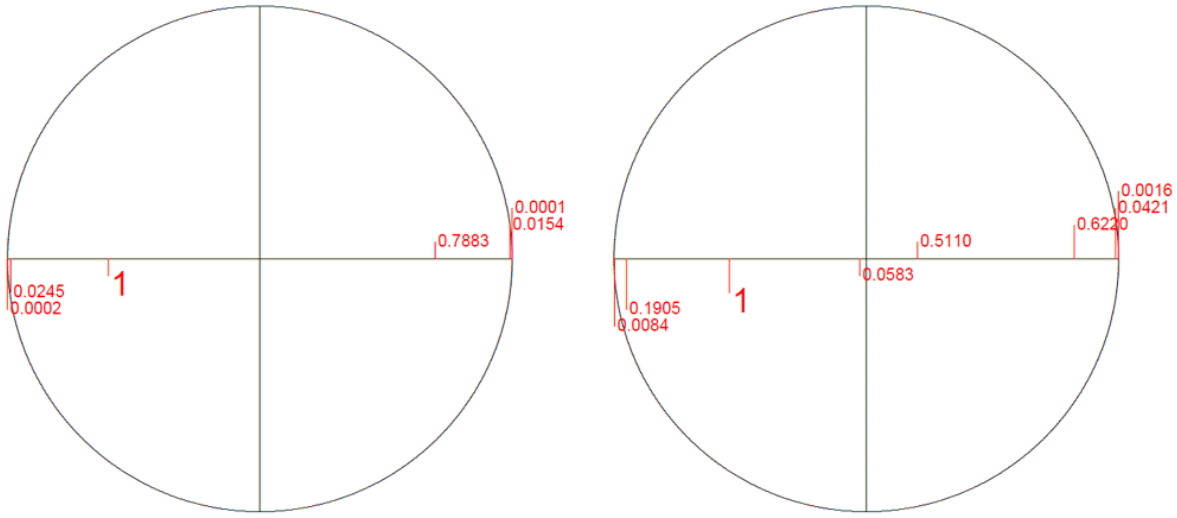

Figure 2: System of images from a single point source in another universe observed through a Bronnikov–Ellis worm hole (a) and a Reissner–Nordstrom black–white hole (b). The circumference radii are h_{max}. The wormhole parameters are $r_g = 0.9r_0$ and $\varphi_1^{tot} = 0.9\pi$. The black–white hole parameters are $Q = 0.6M$ and $\varphi_1^{tot} = 0.5\pi$.

For the maximum impact parameter of a photon in this model that passes from another universe into our Universe, we have $h_{max} = r_m^2/\sqrt{Q^2 - 2Mr_m + r_m^2}$, where $r_m := 1.5M + 0.5\sqrt{9M^2 - 8Q^2}$. Since we have the asymptotics: $\varphi^{tot}(h) \to 2\sqrt{h/Q}$, for $\kappa_{wh}(h) \to \pi hQ/(4l_1^2)$ – see [10].

Figure 2 presents the dependences of the relative brightness $I_{rel}(h)$ of the images[5] for a single star seen from another universe through a wormhole and black–white hole. The vertical lines in this figure mark the places of the first three (four) pairs of visible virtual images, and the corresponding numbers mark the relative brightnesses of these images. The brightnesses of all these images generally turn out to be different; since the brightness of the succeeding pairs of images decreases rapidly starting from the third pair of images, it makes sense to consider no more than the first two pairs of stellar images.

An important conclusion of this section is that all images of a single star observed from another universe through a wormhole lie on the same straight line, while their number (for the main images comparable in brightness) is always greater than one. Therein also lies the fundamental difference from strong gravitational scattering by an ordinary black hole (when

[5] Relative to the brightest image.

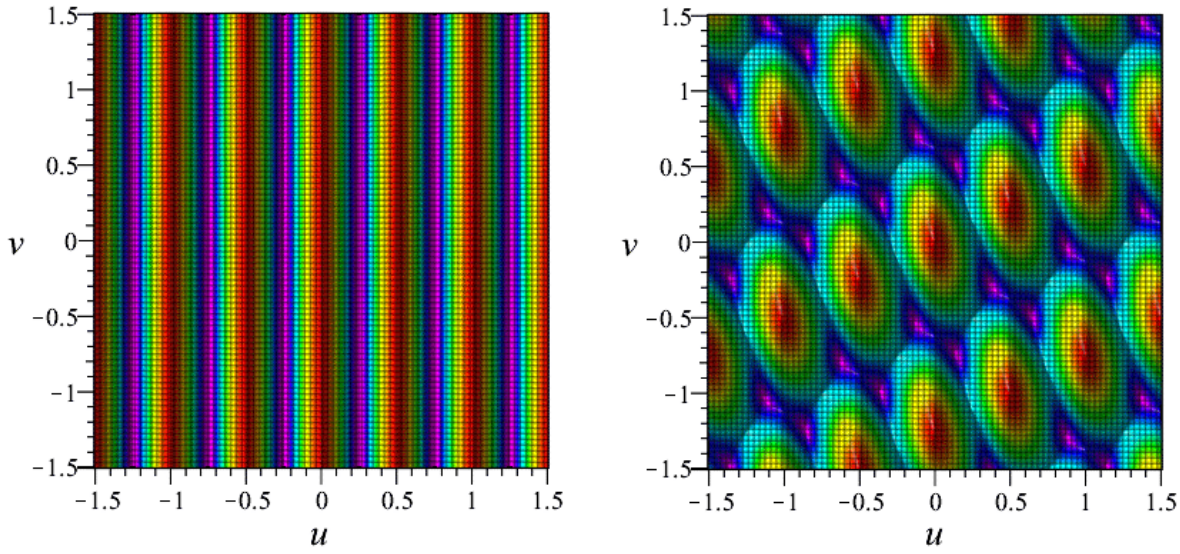

Figure 3: Form of the CFD from several (different) point sources in coordinates (u, v). (a) Two point sources with an angular distance between the sources equal to $2a$ [rad]; the relative brightness of the first and second sources are 2 and 3 arbitrary units, respectively (the latter is a factor of 1.5 brighter). (b) Three point sources (not on a single straight line); their angular coordinates (x_i, y_i) and relative brightnesses I_i are: $x_1 = a$, $y_1 = 0$, $I_1 = 3$; $x_2 = -a$, $y_2 = 0$, $I_2 = 3$; $x_3 = 0.6a$, $y_3 = 0.8a$, $I_3 = 4$. The scale of the unit in coordinates (u, v) corresponds to $\lambda[sm]/(a[rad])$.

the ray of light always remains in our Universe): there will be only one bright image, while the brightness of the remaining images can already be neglected.

IV. MODELING THE IMAGE VISIBILITY AMPLITUDE UNDER GRAVITATIONAL SCATTERING IN A CENTRALLY SYMMETRIC GRAVITATIONAL FIELD

Consider the various cases of modeling sources around a black hole.

Individual point sources are modeled by delta functions: $I_i(x, y) = A_i\,\delta(x - x_i)\,\delta(y - y_i)$. For several point sources, the CFD is then the absolute value of the sum of their Fourier transforms:

$$|V_i(\mathrm{u}, \mathrm{v})| = \left| \sum_i A_i \exp\left[-2\pi i(\mathrm{x_i u} + \mathrm{y_i v})/\lambda\right] \right| \tag{11}$$

1. The model of a single point source. The CFD is a constant: $|V_1(\mathrm{u}, \mathrm{v})| = A_1 = const$.

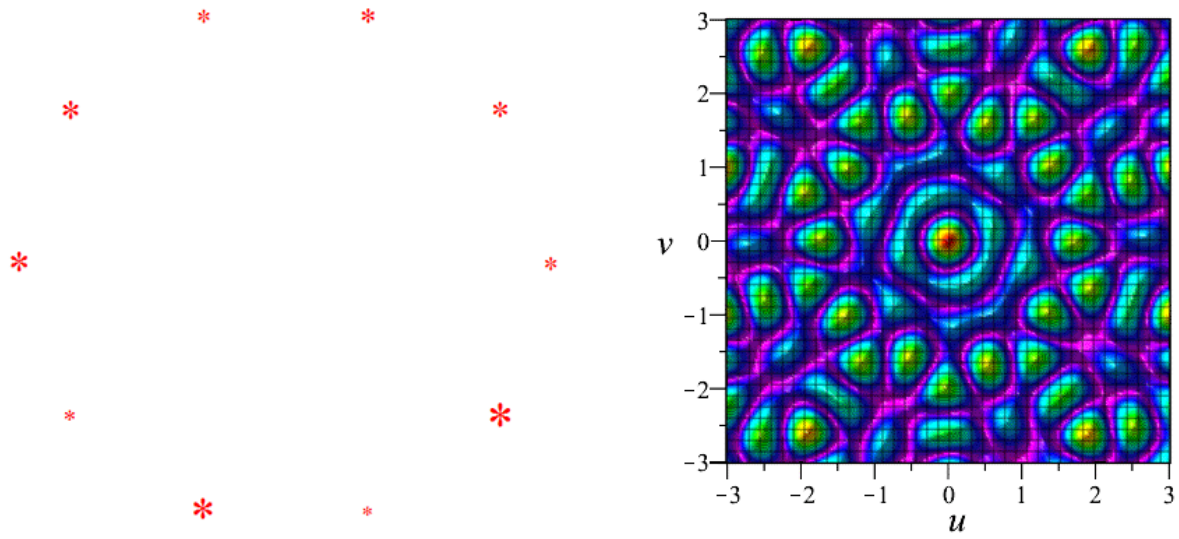

Figure 4: (a) The model of ten comparable (in brightness) point sources that lie on a single circumference with an angular radius R [rad] at equal distances from one another. The relative brightnesses of these sources are: $I_1 = 1$, $I_2 = 0.9$, $I_3 = 0.8$, $I_4 = 1.1$, $I_5 = 1.2$, $I_6 = 0.7$, $I_7 = 1.3$, $I_8 = 0.6$, $I_9 = 1.4$ and $I_{10} = 0.8$. (b) The CFD for this model. The scale of the unit in coordinates (u, v) corresponds to $\lambda[sm]/(R[rad])$.

2. The model of two point sources on a single straight line. The results for this model are displayed in Fig 3a. It can be seen from these results that the point sources located on a single straight line give a characteristic picture for the CFD: the CFD in this case changes only along one direction while remaining constant in an orthogonal direction. It can be shown that this model does not change fundamentally if the number of comparable (in brightness) point sources (on a single straight line) will be greater than two[6]. In this case, the distance between the sources (or the wormhole parameters) can be judged from the periodicity of the CFD change.

3. The model of three point sources that do not lie on a single straight line. The CFD will change in both orthogonal directions, and these changes will also be periodic (see 3b). Again, the mutual distance between the sources can be judged from these periods.

4. The model of ten comparable (in brightness) point sources that lie on a single circumference at equal distances from one another. The CFD for this model

[6] Such a situation is typical for the passage of starlight through a wormhole or black–white hole (several images with a comparable brightness from a single point source lie on a single line; see [10].

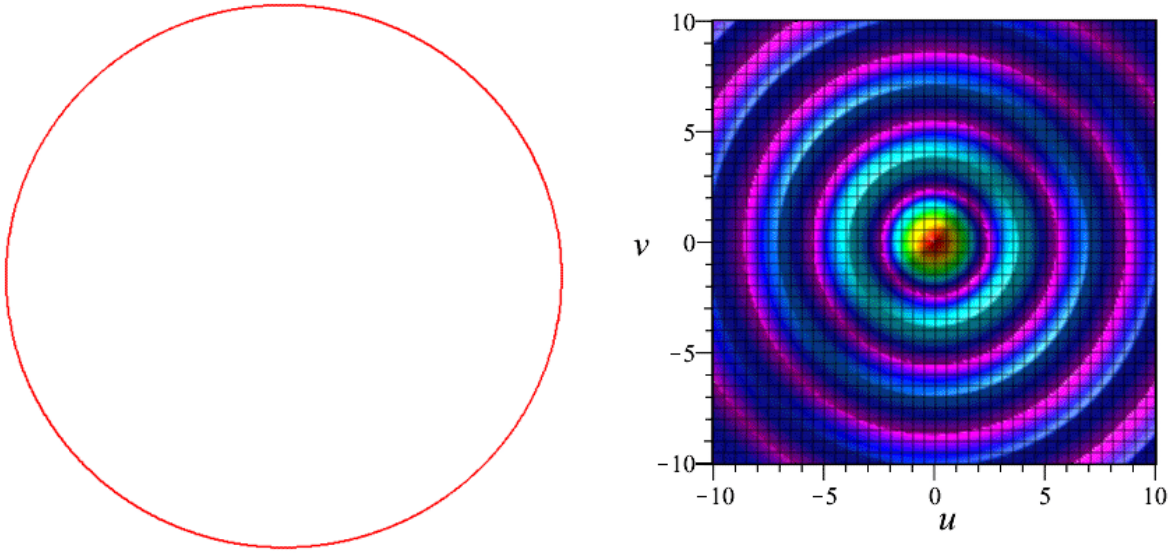

Figure 5: (a) The model of a uniformly shining circumference with an apparent radius r_{ring} [rad]. (b) The CFD of the Fourier transform for this model. The scale of the unit in coordinates (u, v) corresponds to $lambda[sm]/(r_{ring}[rad])$.

is shown in Fig. 4. According to the form of this CFD, it does not matter any longer whether these sources lie on a single circumference or not (at such a number of comparable (in brightness) and equidistant point sources).

5. The model of a uniformly shining circumference. The CFD of the Fourier transform for this model is

$$|V_{ring}(\mathrm{u},\mathrm{v})| = const \cdot |J_0(\eta r_{ring})|\,, \quad \eta := \sqrt{\mathrm{u}^2+\mathrm{v}^2}/\lambda\,. \tag{12}$$

Here $J_p(x)$ – is a Bessel function of order "p" (see. Fig. 5).

6. The crescent model (simulates the model of a non-uniformly shining circumference). Inside a uniformly shining disk with a diameter r_{out} there is a dark disk with a smaller diameter r_{in} displaced from its center (see [7]):

$$|V_{crescent}(\mathrm{u},\mathrm{v})| = \frac{const}{\eta} \cdot \left| r_{out}\, J_1(\eta r_{out}) - e^{-2\pi i(\mathrm{x_c u}+\mathrm{y_c v})/\lambda}\, r_{in}\, J_1(\eta r_{in}) \right| \tag{13}$$

Here, x_c and y_c are the coordinates of the displacement of the inner disk center relative to the outer disk center (see Fig. 6).

7. The crescent model plus two comparable (in brightness) point sources (see

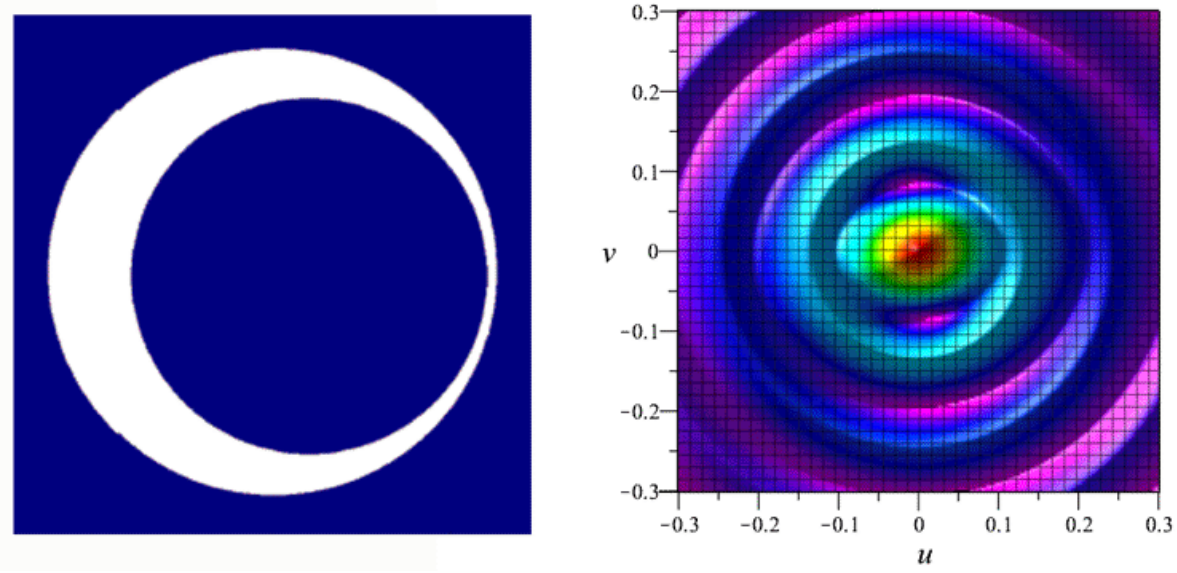

Figure 6: (a) The crescent model (simulates the model of a nonuniformly shining circumference): inside a uniformly shining disk with an apparent diameter r_{out} [rad] there is a dark disk with a smaller diameter displaced from its center; $r_{in} = 0.8r_{out}$, $x_c = 0.16r_{out}$ and $y_c = 0.02r_{out}$. (b) The CFD of the Fourier transform for this model. The scale of the unit in coordinates (u, v) corresponds to $\lambda[sm]/(r_{out}[rad])$.

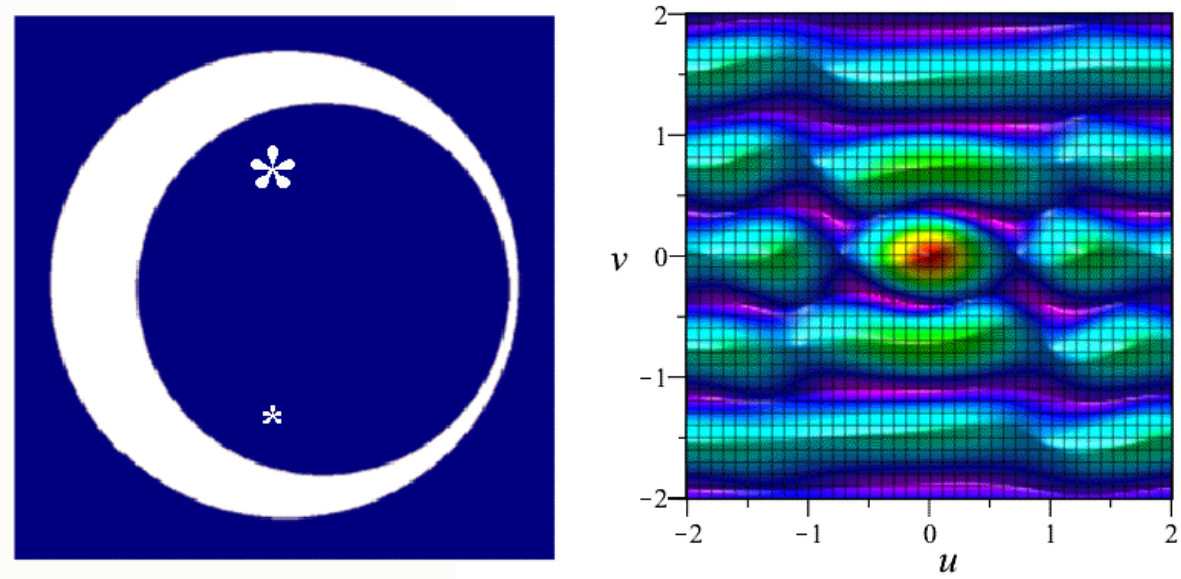

Figure 7: (a) The crescent model, $r_{in} = 0.8r_{out}$ (see Fig. 6), with weight $A_0 = 1$ (and a corresponding brightness $\approx 1.13r_{out}^2$) plus two comparable (in brightness) point sources with weights $A_1 = 0.1$, $A_2 = 0.05$ and coordinates $y_1 = 0.6r_{out}$, $y_2 = -0.7r_{out}$ (see (14)). (b) The CFD of the Fourier transform for this model. The scale of the unit in coordinates (u, v) corresponds to $\lambda[sm]/(r_{out}[rad])$.

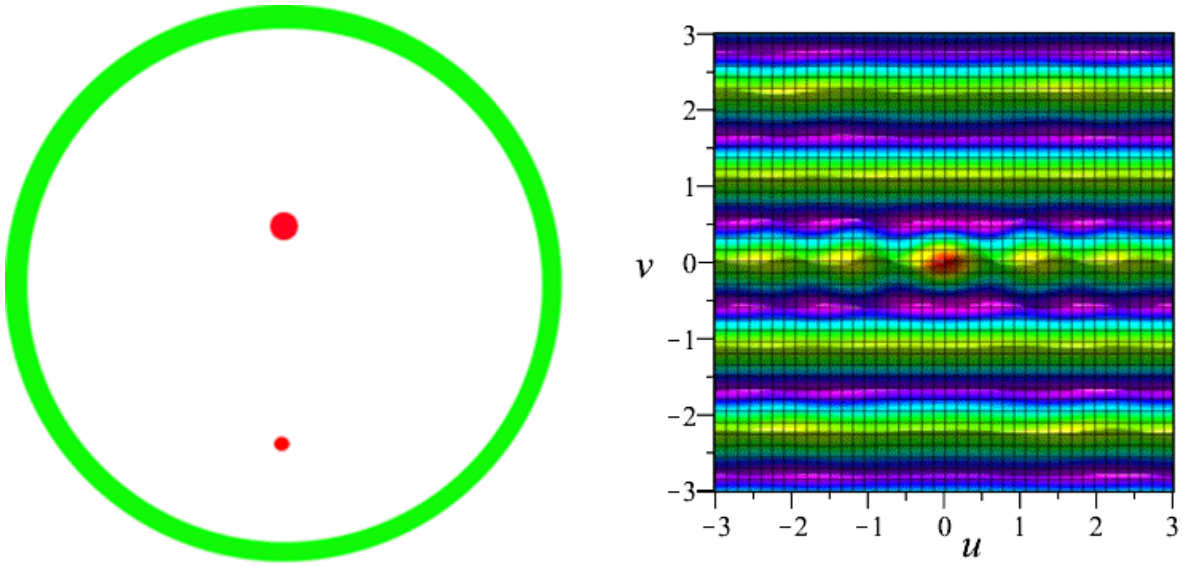

Figure 8: (a) The model of a thick circumference plus two oppositely displaced point sources with the same total brightness $I_{ring} = 1$. The coordinates of the sources are $y_1 = +0.2r_{out}$ and $y_2 = -0.7r_{out}$; the relative brightnesses of the sources are $I_1 = 0.8$ and $I_2 = 0.2$. (b) The CFD for this model. The scale of the unit in coordinates (u, v) corresponds to $\lambda[sm]/(r_{out}[rad])$.

Fig. 7). We have

$$|V_{crescent+points}(\mathrm{u},\mathrm{v})| = \left| \frac{A_0}{\eta} \left[r_{out}\, J_1(\eta r_{out}) - e^{-2\pi i(\mathrm{x_c u + y_c v})/\lambda}\, r_{in}\, J_1(\eta r_{in}) \right] + \sum_j A_j e^{-2\pi i (y_j \mathrm{v})/\lambda} \right| \quad (14)$$

It is important to compare the relative brightnesses of the crescent and the point source in this model. Therefore, we will assume that a unit brightness, the brightness of a 1x1 area with a unit weight, corresponds to the delta function (i.e., a point source with a unit weight). The brightness of the crescent with a unit weight will then be $\pi(r_{out}^2 - r_{in}^2)$.

8. The model of a thick circumference plus two oppositely displaced point sources with the same total brightness (see Fig. 8):

$$|V_{ring+points}(\mathrm{u},\mathrm{v})| = A_1 \left| \frac{r_{out}\, J_1(\eta r_{out}) - r_{in}\, J_1(\eta r_{in})}{\eta\, r_{out}^2} + I_1 e^{-2\pi i y_1 \mathrm{v}/\lambda} + (1 - I_1) e^{-2\pi i y_2 \mathrm{v}/\lambda} \right| \quad (15)$$

The brightness of the thick circumference and the total brightness of both point sources in the model are chosen to be the same. For this purpose, we assume that $r_{in} := r_{out}\sqrt{1 - 1/\pi}$ and $I_1 \in [0,\, 1]$.

In this model, it is also important to determine the minimum ratios y_1/r_{out} and y_2/r_{out} at which the visual asymmetry of the picture is still seen.

V. ASYMMETRY OF THE CORRELATED FLUX DENSITY

As has become clear from the previous section, one of the characteristic features in the CFD when wormholes or black–white holes are observed can be its asymmetry in coordinates (u, v). Therefore, it makes sense to introduce a measure of this asymmetry. Suppose that the model under consideration is completely symmetric with the center of symmetry at the coordinate origin on the (u, v)-plane. For any two rays on this plane originating from the coordinate origin, the CFD will then be identical at equal distances from the center. The asymmetry in this case is zero, as, for example, in models 1 and 5 considered in the previous section.

Let us define the degree of asymmetry As as

$$As := \frac{max\{Int(\tau)\} - min\{Int(\tau)\}}{max\{Int(\tau)\} + min\{Int(\tau)\}}, \quad Int(\tau) := \int\limits_0^{+\infty} \left| \frac{d|V(\eta,\tau)|}{d\eta} \right| d\eta. \tag{16}$$

Here, we have introduced the polar coordinate (η, τ) instead of the Cartesian coordinates (u, v):

$$\mathrm{u}(\eta,\tau) := \lambda\eta \cdot \cos(\tau), \quad \mathrm{v}(\eta,\tau) := \lambda\eta \cdot \sin(\tau). \tag{17}$$

For this definition, the maximum possible degree of asymmetry is equal to one: $max\{As\} = 1$. The degree of asymmetry for models 2, 3, 4, 6, 7, and 8 lies within the range $0 < As < 1$. We numerically calculated the asymmetry for two of these models:

Model 6: $As^6 \approx 0.47$ at $x_c = 0.2r_{out}$, $y_c = 0$ and $As^6 \approx 0.36$ at $x_c = 0.1r_{out}$;

Model 8: $As^8 \approx 0.13$ at $y_1 = +0.2r_{out}$, $y_2 = -0.7r_{out}$ and $a_1 = 0.8$.

For models 6 and 8, we took a finite range of integration[7], $\eta \in [0,\ 10]$, when calculating the asymmetry in integral (16).

As can be seen from these data, model 6 possesses an even greater asymmetry than model 8 for such a definition. However, model 6 is also used to describe the shadow from the black hole (see [7]). Therefore, it is impossible to unambiguously distinguish the effects related to non-central point sources from other effects (related, for example, to ordinary black holes) based only on the asymmetry (16) in the range of integration $\eta \in [0,\ 10]$.

[7] Note that $Int(\tau)$ does not depend on the units of measurement of λ, because the scale factor cancels out after integration.

To improve our method, let us modify Eq. (16) in such a way that the analogous effects from other objects (for example, from ordinary black holes) are excluded in the asymmetry determination. For this purpose, notice that only the CFD oscillations associated with the pair point sources that lie on a single straight line with the coordinate origin make a major contribution to the asymmetry at great distances from the coordinate origin. This is just what we need to describe the pair of images from a single point source when observed through a wormhole or black–white hole. Therefore, to reveal the sought-for effects (precisely from such point sources) in the asymmetry, let us modify one of Eqs. (16):

$$Int_{mod}(\tau) := \int\limits_{\eta_1}^{\eta_2} \left| \frac{d|V(\eta,\tau)|}{d\eta} \right| d\eta, \tag{18}$$

where $1 << (\eta_2 - \eta_1) << \eta_1 < \eta_2$. In such a modified case, we obtain the following values for models 6 and 8 for the parameters $\eta_1 = 100$ and $\eta_2 = 110$:

model 6: $As^6_{mod} \approx 0.30$ at $x_c = 0.2r_{out}$, $y_c = 0$ and also at $x_c = 0.1r_{out}$;

model 8: $As^8_{mod} \approx 0.93$ at $y_1 = +0.2r_{out}$, $y_2 = -0.7r_{out}$ and $a_1 = 0.8$.

Thus, the asymmetry in the modified definition (18) dominates and approaches unity in the cases of interest to us: when pair point sources that lie on a single straight line with the coordinate origin are present in the image. Of course, the specific value of As_{mod} depends on the choice of $\eta_1 < \eta_2$, but we are interested only in the closeness of As_{mod} to unity to distinguish the different possible topologies of the observed object.

VI. DISCUSSION

It is clear from what has been said above that unambiguous conclusions cannot always be drawn from the form of the CFD distribution function alone.

For example, it will be difficult to determine in practice whether the numerous point sources are located on a circumference or they are distributed inside it from the form of the CFD distribution (in Fig. 4).

The crescent model considered above can also correspond to different physical situations: for example, the model of a non-uniformly shining circumference (see Fig. 6) or the model of an accretion disk that is shadowed by a black hole on one side. In this case, the "blurred" crescent model (to allow for the interstellar scattering effects; see, e.g., [7]) is used for the best agreement with the observations. Various kinds of blurring are also often applied in

other models. All of this makes numerous simulations of such a kind difficult to distinguish from one another.

However, the models where there are distributions of sources along a single straight line (see Figs. 3, 7 and 8)) constitute an important exception from the aforesaid. In these cases, a characteristic feature of such models is the existence of a direction on the (u, v) plane in which the CFD remains constant (at great distances from the center). It is these cases that are particularly interesting for the detection of wormholes and black–white holes (see, [10]).

The combination (superposition) of models 2 and 6, whose results are presented in Fig. 7, is some intermediate case (model 7). Signatures that will more likely be typical of a wormhole or black–white hole can also be revealed here. It is important that a periodicity in coordinate v (in the absence of a distinct periodicity in coordinate u) is still clearly visible even at a crescent brightness that is greater than the total brightness of the point sources by approximately seven and a half times. Thus, this model has a stable signature of a black–white hole or wormhole. This signature manifests itself more and more as one recedes from the center, because the CFD of the crescent (or a different brightness distribution symmetric in angle τ) decreases as $\propto \eta^{-3/2}$, while the CFD of pair point sources with a comparable brightness oscillates with a constant amplitude and, as a result, its contribution becomes dominant.

Model 8 shows that the presence of pair sources that lie on a single straight line with the coordinate origin in the image changes radically the situation. Such a model (just as model 7) will possess an asymmetry close to unity! Detecting this signature will allow one to talk about the discovery of an object like a wormhole or black–white hole. This will be possible if the angular distance between the pair sources in the model will be less than or of the order of the angular size of the horizon diameter for the corresponding black hole. However, the presence of a sufficiently bright source in another universe whose photons (coming to us) would produce a system of pair images (see Fig. 2) is also needed for this condition to be realized. In this case, the pairs of such images will satisfy the condition corresponding to Fig. 8 and $As_{mod} \approx 1$.

Note that in this paper we have considered the case of a monochromatic radiation spectrum and a certain relation between the flux densities from different image details (for more details, see Section IV). The CFD form that we presented for various characteristic cases can vary as these assumptions change. The models considered here are directly applicable only in the case of a sufficiently high telescope resolution in recorded spectral band width

$\Delta\lambda/\lambda$. This condition, $\Delta\lambda/\lambda << 1$, is met for VLBI systems. However, $\Delta\lambda/\lambda \sim 0.2$ for optical and infrared interferometers. Therefore, an assumption about the radiation spectra of image details in the detected band $\Delta\lambda$ should be made to apply our models in the optical and infrared ranges.

---

[1] A. R. Thompson, J. M. Moran, and G. W. Swenson, Jr., *Interferometry and Synthesis in Radio Astronomy, 2nd Edition* (Wiley, 2001).

[2] K. I. Kellermann and J. M. Moran, ARA&A **39**, 457 (2001).

[3] A. Quirrenbach, ARA&A **39**, 353 (2001).

[4] A. Quirrenbach, ISSI Scientific Reports Series **9**, 293 (2010).

[5] R.-S. Lu, A. E. Broderick, F. Baron, J. D. Monnier, V. L. Fish, S. S. Doeleman, and V. Pankratius, ApJ **788**, 120 (2014).

[6] N.S. Kardashev, N.S. Kardashev, V.V. Khartov, et al., Astron. Rep. **57 (3)**, 154 (2013).

[7] A.B. Kamruddin and J. Dexter, MNRAS **434**, 765 (2013).

[8] A.E. Broderick and A. Loeb, ApJ **697**, 1164 (2009).

[9] F. Eisenhauer et al., ApJ **598**, 121—124 (2003).

[10] N.S. Kardashev, L.N. Lipatova, I.D. Novikov, and A.A. Shatskii, J. Exp. Theor. Phys. **119 (1)**, 63 (2014).

[11] A.F. Zakharov, *Gravitational Lenses and Microlenses* (Yanus-K, Moscow [in Russian], ISBN 5-88929-037-1, 1997).

[12] L.D. Landau and E.M. Lifshitz, *Course of Theoretical Physics, Volume 2: The Classical Theory of Fields* (Nauka, Moscow, 1988, Butterworth–Heinemann, Oxford, 1991).

[13] Alexander Shatskiy, Phys.—Usp. **52 (8)**, 811 (2009).

[14] H. G. Ellis, J. Math. Phys. **14**, 104 (1973).

[15] K. A. Bronnikov, Acta Phys. Pol. B **4**, 251 (1973).